

## Electronic Supporting Information

### Functionalized Thiazolidone Decorated Lanthanum Doped Copper oxide: Novel Heterocyclic Sea Sponge Morphology Conducting Efficient Detection of Dopamine

Umay Amara,<sup>1,2</sup> Khalid Mahmood,<sup>\*1</sup> Maria Hassan,<sup>1</sup> Muhammad Hanif,<sup>3</sup> Muhammad Khalid,<sup>5</sup> Muhammad Usman,<sup>4</sup> Zahid Shafiq,<sup>1</sup> Usman Latif,<sup>2</sup> Muhammad Mahboob Ahmed,<sup>1</sup> Akhtar Hayat,<sup>2</sup> Mian Hasnain Nawaz<sup>\*2</sup>

<sup>1</sup> *Institute of Chemical Sciences, Bahauddin Zakariya University, Multan 60800, Pakistan*

<sup>2</sup> *Interdisciplinary Research Centre in Biomedical Materials (IRCBM), COMSATS University Islamabad, Lahore Campus 54000, Pakistan*

<sup>3</sup> *Department of Pharmacy, Bahauddin Zakariya University, Multan 608000, Pakistan*

<sup>4</sup> *Institute of Biomedical Materials and Engineering, College of Materials Science and Engineering, Qingdao University, 308 Ningxia Road, Qingdao, Shangdong 266071, China*

<sup>5</sup> *Department of Basic Sciences & Humanities, Khwaja Fareed University of Engineering & Information Technology, Rahim Yar Khan 64200, Pakistan*

<sup>6</sup> *Department of Chemistry, COMSATS University Islamabad, Lahore Campus 54000, Pakistan*

Correspondence: (K.M.) khalidmahmood@bzu.edu.pk ; (M.H.N.) mhnawaz@cuilahore.edu.pk

#### 1. Experimental SeDMTOx

##### 1.1. Chemicals

Copper (II) nitrate trihydrate, sodium hydroxide, lanthanum nitrate hexahydrate, isatin, bromoacetic acid, N,N'-aryl-acyl thiourea, and sodium acetate, potassium ferrocyanide ( $K_4Fe(CN)_6$ ), dimethyl formamide (DMF), fructose, potassium ferricyanide ( $K_3Fe(CN)_6$ ), ethanol, phosphate buffer saline (PBS), dopamine, glucose, urea, ascorbic acid, uric acid, L-cysteine, were bought from Sigma-Aldrich and were used as received. Tear sample was obtained voluntarily and saved at 4°C. All other chemicals were of good analytical grade and solutions were prepared at room temperature from doubly distilled water by Milli-Q water purifying system.

## 1.2. Instrumentation

Electrochemical experiments were conducted at Gamry 1010 interface. The three-electrode system with graphitic pencil electrode (GPE) as a working electrode, Ag/AgCl/Sat. KCl utilized as a reference electrode with standard potential of ( $E=+0.197$  Vs saturated) and platinum-containing counter electrode has been exploited. Electrochemical Impedance Spectroscopy (EIS) measurements were executed in the presence of 5 mM ferro/ferri solution (1:1). Fourier Transform Infrared (FTIR) spectrums were recorded on Thermo scientific Nicolet 6700 in the ATR modulation to study the functional groups exist in the pristine, doped and hybrid material. X-ray diffraction (XRD) measurements has been employed to analyze phase composition utilizing a Rigaku D/max-2550 apparatus equipped with a Cu-K $\alpha$  radiation source ( $\lambda=1.5418$  Å). Raman spectrum was recorded on Renishaw in Via-reflex spectrometer. The surface morphology of fabricated interfaces were studied by scanning electron microscopy (SEM) at TESCAN VEGA 3. Working interface i.e. GPE was manually cut using cutter and exploited for microscopic analysis.

## 1.3. Real sample analysis Sample Preparation

To assess the practical application of developed sensor, spiked tear samples were analyzed against DA. The tear samples were obtained voluntarily from patient in eppendorf and stored at 4 °C. Primarily, the obtained tear sample (500  $\mu$ L) was diluted with (500  $\mu$ L) of PBS buffer pH (7.4). To obtain the desired analyte concentrations, the stock solution was prepared by mixing 5 mM DA solution (1000  $\mu$ L) + diluted tear solution (1000  $\mu$ L). The recovery experiments were performed by adding aliquots from the freshly prepared stock solution.

The contents of the solutions are listed below.

20  $\mu$ M= (80  $\mu$ L aliquot from stock + 20 mL PBS)

50  $\mu$ M= (200  $\mu$ L aliquot from stock + 20 mL PBS)

100  $\mu$ M= (400  $\mu$ L aliquot from stock + 20 mL PBS)

300  $\mu$ M= (1200  $\mu$ L aliquot from stock + 20 mL PBS)

Finally, for analysis DPV was performed on La@CuO-DMT/GPE based sensor.

$$\text{Recovery \%} = 100 - \text{Relative Error} \quad (S1)$$

## 2. Results and Discussion

Limit of detection (LOD)

The LOD was calculated using equation S2.

$$\text{LOD} = F \cdot \frac{SD}{b} \quad (S2)$$

Wherein,

F represents factor of 3.3, SD represents Standard deviation of the blank sample, ordinate intercept, or residual of the linear regression which is 0.1 and b corresponds to the Slope of regression line.

Meanwhile Sensitivity can be calculated using equation S3.

$$\text{Sensitivity} = \frac{\text{Current}}{\text{Analyte concentration} \cdot \text{Electrode area}} \quad (S3)$$

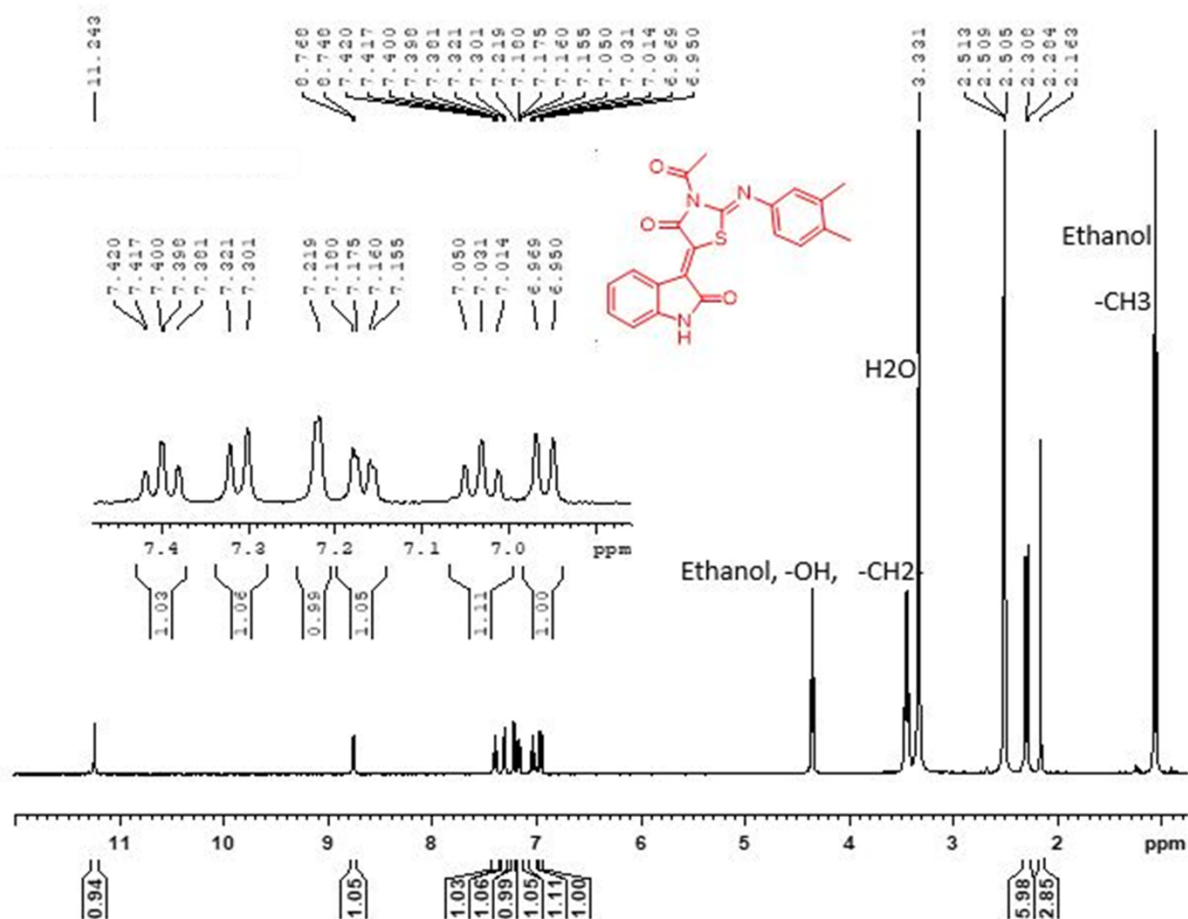


Fig S1. <sup>1</sup>H NMR of DMT.

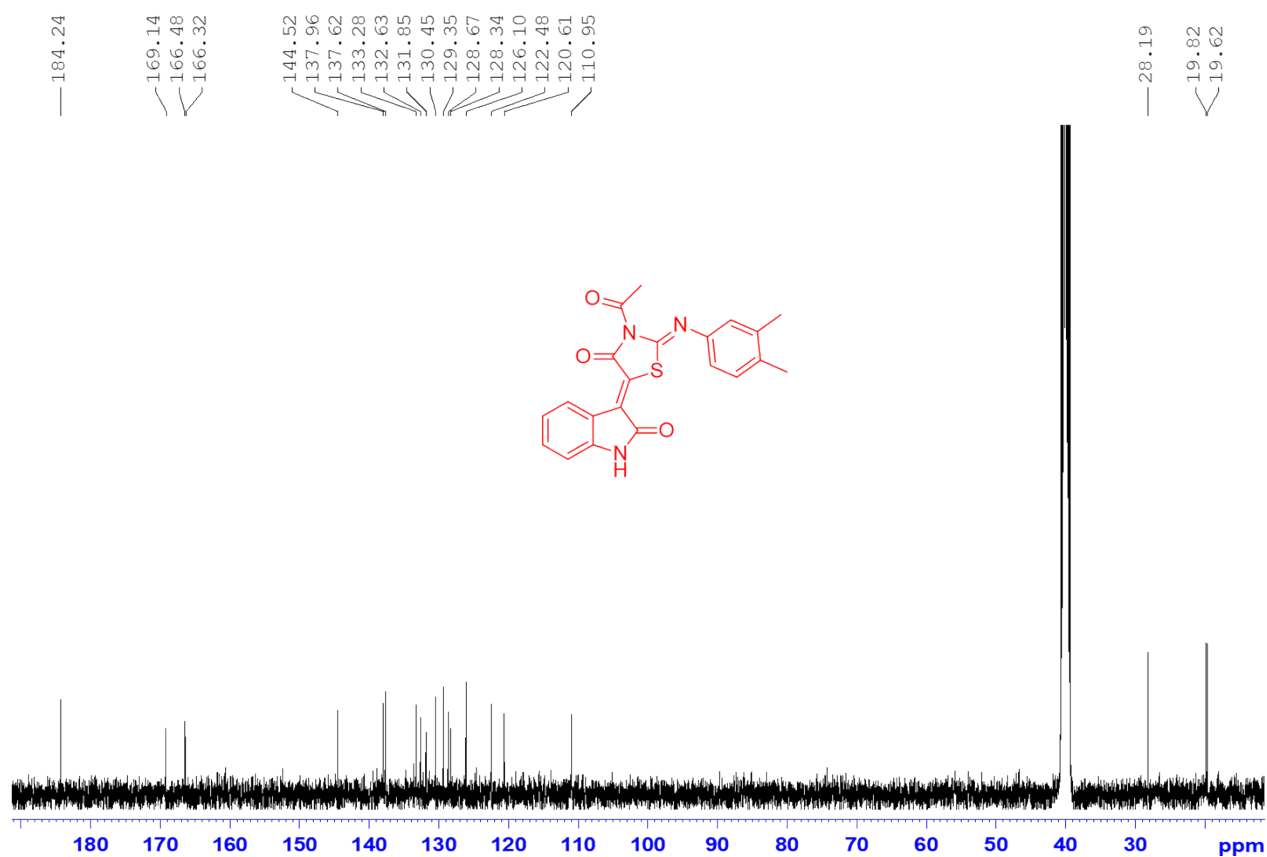
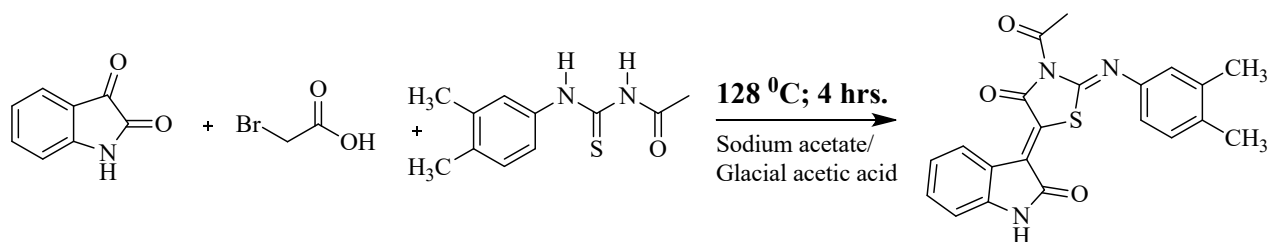


Fig S2. <sup>13</sup>C NMR of DMT.

<sup>1</sup>H-NMR  $\delta$  ppm: 2.30(s,6H,CH<sub>3</sub>), 7.18 (s, 1H), 7.15 (dd,  $J$  = 8 Hz, 1H), 6.95 (d,  $J$  = 7.6, 1H), 7.17 (t,  $J$  = 8Hz, 1H), 7.41 (td, 1H), 7.03 (td, 1H), 7.32 (dd,  $J$  = 7.32, 1H), 11.24 (s, 1H, NH isatin, D<sub>2</sub>O exchangeable). <sup>13</sup>C NMR  $\delta$  ppm: 184.24, 169.24, 166.48, 166.32, 144.52, 137.96, 137.62, 133.28, 132.63, 131.85, 130.45, 129.35, 128.67, 128.34, 126.10, 122.48, 120.65, 110.95, 28.19, 19.82,19.62.



Scheme S1. Knoevenagel condensation reaction between 1H-indole-2,3-dione, bromoacetic acid and aryl-acyl thiourea to form target conjugate.

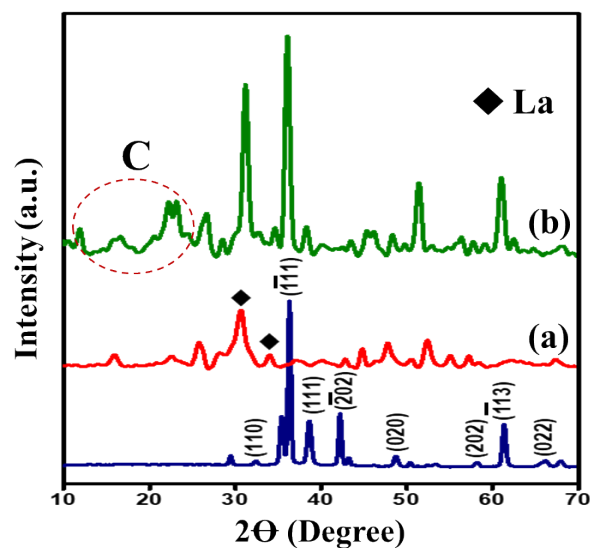


Fig S3. XRD pattern of (a) CuO; (b) La@CuO; (c) La@CuO-DMT.

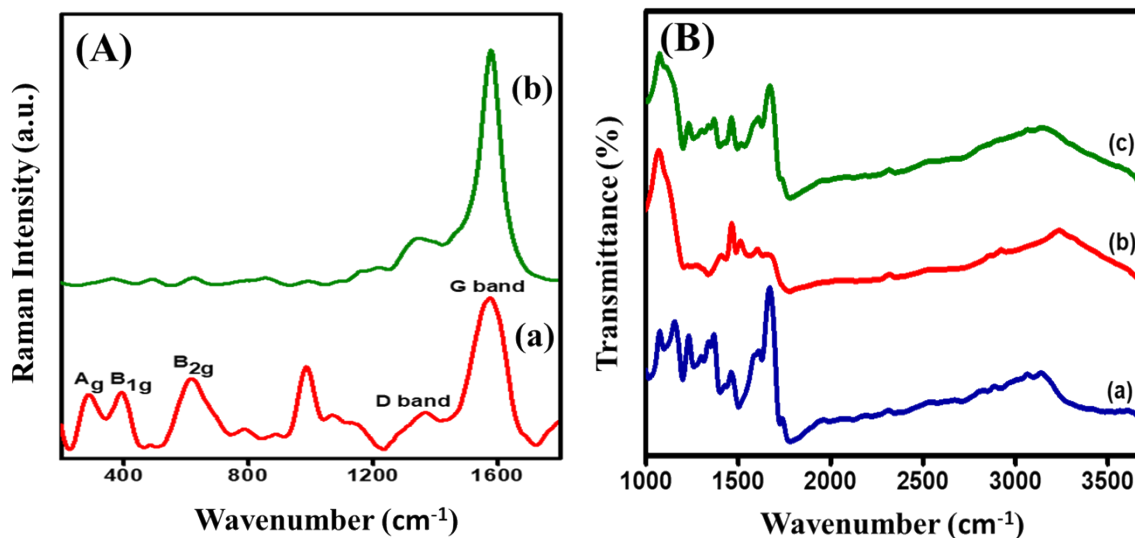


Fig S4. Raman (A) of (a) La@CuO; (b) La@CuO-DMT and FTIR (B) of (a) DMT; (b) La@CuO; (c) La@CuO-DMT.

Molecular structure of DMT, La@CuO and La@CuO-DMT has been examined via FTIR as shown in Fig. S1B. The absorption peak at  $3136\text{ cm}^{-1}$  is credited to stretching frequency of N–H group of core DMT, and the band between  $2808\text{ cm}^{-1}$  and  $2822\text{ cm}^{-1}$  are owed to the stretching frequency of the C–H bond of the aliphatic side chains. A characteristic band at  $1664\text{ cm}^{-1}$  is due

to the carbonyl stretching frequency. Besides, strong absorption bands at 1608 and 1454 are due to C=C and C-C of DMT as revealed in Fig. S4B(a). Meanwhile, the weak absorption at 3256  $\text{cm}^{-1}$  is due to O-H stretching of absorbed moisture. The band at 1681  $\text{cm}^{-1}$  is due to physisorbed carbon dioxide on CuO. The bands below 1200  $\text{cm}^{-1}$  are because of monoclinic phase of CuO.<sup>1</sup> A prominent broadband of La@CuO at 1098  $\text{cm}^{-1}$  credited to the multi-phonon band due to the local density of anisotropic carriers<sup>2</sup> as shown in Fig. S4B(b) and discussed previously in XRD findings. However, the mixed bands has been observed in La@CuO-DMT, illustrating the hybrid formation due to  $\pi$ - $\pi$  interactions between these pristine materials as shown in Fig. S4B(c).

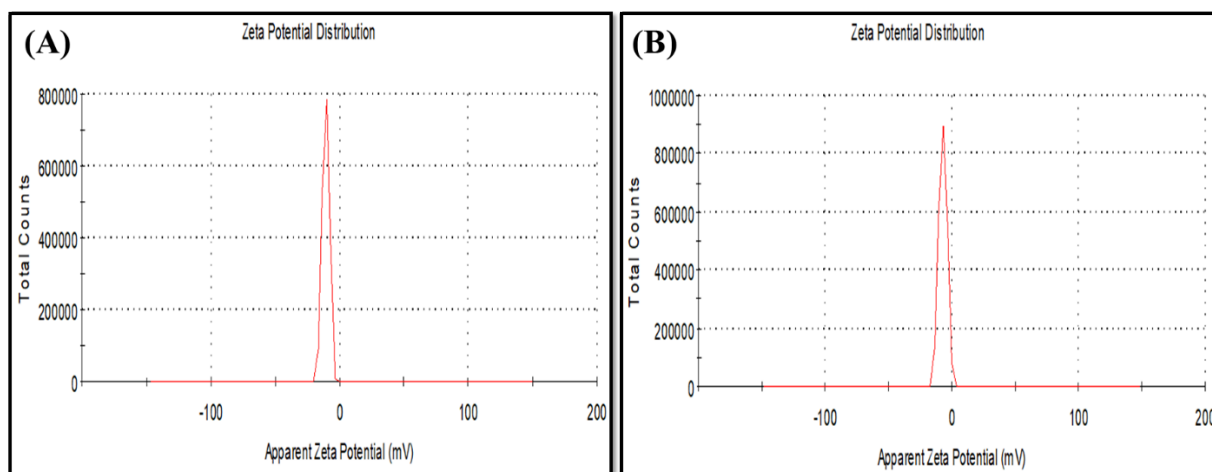


Fig S5. Zeta potential of (A) CuO and (B) La@CuO.

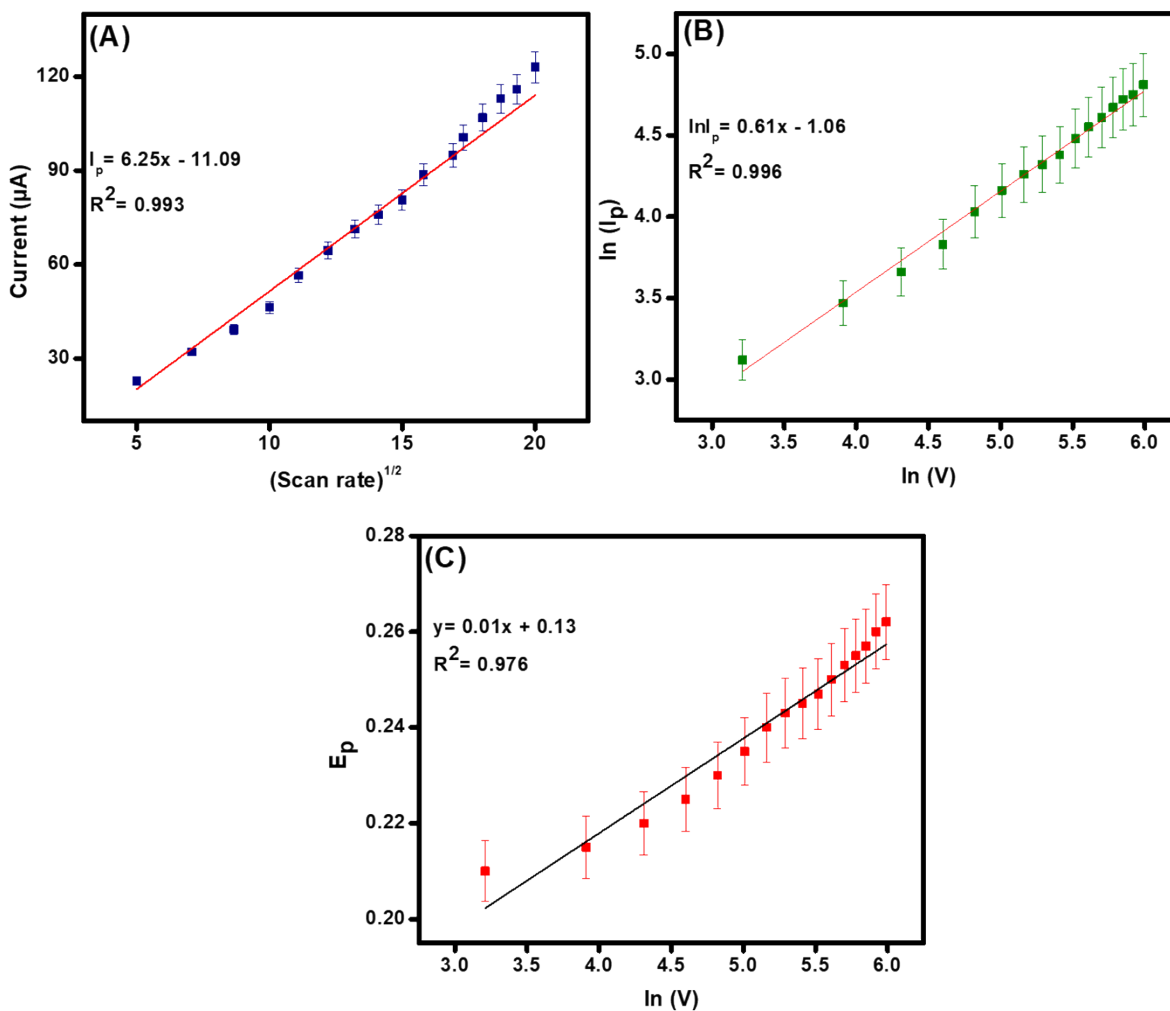


Fig S6. Graph (A) reveal a linear relationship between anodic peak current versus scan rate and the oxidative peak current against square root of scan rate, (B) shows a linear relation between the natural log of scan rate versus natural log of anodic peak current. Graph (C) showing relationship between the natural log of scan rate versus peak potential.

$$y = 0.28v \left( \frac{mV}{s} \right) + 17.42 \quad (R^2 = 0.996) \quad (S4)$$

Further, a linear relationship was obtained between the square root of scan rate vs anodic current as could be witnessed from Fig. S6(A), proposing a diffusion controlled process. It could be accredited to the active surface area of La@CuO-DMT, resulting in enhanced electron transfer kinetics.

$$I_p = 6.25v \left( \frac{mV}{s} \right) - 11.9 \quad (R^2 = 0.993) \quad (S5)$$

Meanwhile, a linear regression equation was also achieved by plotting a graph between the natural log of scan rates versus anodic peak currents, as shown in Fig. S6(B).

$$\ln I_p = 0.61v\left(\frac{mV}{s}\right) - 1.06 \quad (R^2 = 0.996) \quad (S6)$$

In addition, a graph plotted between the peak potential ( $E_p$ ) versus natural log of scan rate resulted a linear relationship, as shown in Fig. S6(C).

$$E_p = 0.01 \ln v + 0.13 \quad (R^2 = 0.976) \quad (S7)$$

Table S1: The recovery data of the designed sensor in tear samples for DA analysis (n= 3).

Sample No.	Sample added ( $\mu\text{M}$ )	Sample Found ( $\mu\text{M}$ )	Recovery %
1	20	19.9	99.5
2	50	47.5	96
3	100	102.5	97.4
4	300	284.3	105.2

Table S2. Comparison of various sensors developed for DA detection with our designed La@CuO-DMT/GPE.

Electrode Material	LOD (nM)	Sensitivity ( $\mu\text{A} \cdot \mu\text{M}^{-1} \text{cm}^{-2}$ )	Reproducibility (RSD %)	Linear range ( $\mu\text{M}$ )	Ref.
PDI-MXene/GPE	31	9.61	1.9	10-2000	3
GCE/N-rGO-180 8/NH <sub>3</sub>	410	1.82	6.22	0.5–150	4
Nb <sub>2</sub> C MXene/ZnS	1390	12.1		90-820	5
SiTi/AuNP/CPE	570	0.074	5.19	20-180	6
H-ZIF/GCE	12	0.32	5.5	0.25-590	7
Ag@MoS <sub>2</sub> /GCE	200	-	-	1-500	8
RuS <sub>2</sub> /GCE	78.3	1.8	6.4	10–80	9
pS-BIL MIP PeGE	130	-	-	0.5-250	10
CdSe/CdS MSQDs	96	-	7.2	0.5-15	11
La@CuO-DMT/GPE	423	13.9	1.01	10-1500	This Work

PDI-MXene/GPE= Perylene diimide decorated Mxene/Graphitic Pencil electrode; N-rGOs= Nitrogen doped reduced graphene oxides; Nb<sub>2</sub>C MXene/ZnS = Niobium carbide/Zinc sulphide; SiTi/AuNP= silica-titania/gold nanoparticles; H-ZIF= hollow zeolitic imidazolate; Ag@MoS<sub>2</sub>= Molybdenum Disulfide Nanosheet fabricated with Silver Nanoparticles; RuS<sub>2</sub>/GCE= ruthenium(IV) disulfide/glassy carbon electrode; pS-BIL NIP= electrochemically formed thianbilan molecularly imprinted polymer; MSQDs= magic-sized quantum dots.

## References

1. A. Badawi, S. S. Alharthi, M. Althobaiti, A. N. Alharbi, H. Assaedi, H. I. Alkhamash and N. Al-Hosiny, *Applied Physics A*, 2021, **127**, 1-9.
2. J. D. Rodney, S. Deepapriya, M. C. Robinson, C. J. Raj, S. Perumal, B. C. Kim and S. J. Das, *International Journal of Hydrogen Energy*, 2020, **45**, 24684-24696.
3. U. Amara, M. T. Mehran, B. Sarfaraz, K. Mahmood, A. Hayat, M. Nasir, S. Riaz and M. H. Nawaz, *Microchimica Acta*, 2021, **188**, 1-13.
4. P. Wiench, Z. González, R. Menéndez, B. Grzyb and G. Gryglewicz, *Sensors and Actuators B: Chemical*, 2018, **257**, 143-153.
5. N. Arif, S. Gul, M. Sohail, S. Rizwan and M. Iqbal, *Ceramics International*, 2021, **47**, 2388-2396.
6. F. de Matos Morawski, B. B. Xavier, A. H. Virgili, K. dos Santos Caetano, E. W. de Menezes, E. V. Benvenutti, T. M. H. Costa and L. T. Arenas, *Materials Science and Engineering: C*, 2021, **120**, 111646.
7. Y. Dong, J. Liu and J. Zheng, *Colloids and Surfaces A: Physicochemical and Engineering Aspects*, 2021, **608**, 125617.
8. M. Sookhakian, W. J. Basirun, B. T. Goh, P. M. Woi and Y. Alias, *Colloids and Surfaces B: Biointerfaces*, 2019, **176**, 80-86.
9. J. Deepika, R. Sha and S. Badhulika, *Microchimica Acta*, 2019, **186**, 480.
10. H. K. Kaya, S. Cinar, G. Altundal, Y. Bayramli, C. Unaleroglu and F. Kuralay, *Sensors and Actuators B: Chemical*, 2021, 130425.
11. C. C. L. de França, D. Meneses, A. C. A. Silva, N. O. Dantas, F. C. de Abreu, J. M. Petroni and B. G. Lucca, *Electrochimica Acta*, 2021, **367**, 137486.